Master's Degree Thesis
ISRN: HK/R-IMA-EX--1997/D-02--SE

Dynamic Behaviour of a Soil Compaction Tamping Machine

Jens Borg

Anders Engström

Department of Mechanical Engineering
University of Karlskrona/Ronneby
Karlskrona, Sweden

1997

Supervisor: Göran Broman, Ph.D. Mech. Eng.

Dynamic Behaviour of a Soil Compaction Tamping Machine

Jens Borg

Anders Engström

Department of Mechanical Engineering

University of Karlskrona/Ronneby

Karlskrona, Sweden

1997

Thesis submitted for completion of Master of Science in Mechanical Engineering with emphasis on Structural Mechanics at the Department of Mechanical Engineering, University of Karlskrona/Ronneby, Karlskrona, Sweden.

Abstract:
A theoretical model was suggested and equations of motion derived. A computer program was developed to solve the resulting system of equations. Agreement between calculated and experimental results is not quite satisfactory. Reasons for discrepancy are discussed and suggestions for further investigation are given.

Keywords:
Dynamic, Compaction, Tamper, Theoretical model, Experimental verification.

Acknowledgements

This work was carried out at the Department of Mechanical Engineering, University of Karlskrona/Ronneby, Karlskrona, Sweden, under the supervision of Dr. Göran Broman.

We wish to thank Dr. Göran Broman for his guidance and advice, which helped us a lot.

At the Department of Analysis and Test, Svedala Compaction Equipment AB, Karlskrona, Sweden, we wish to thank M.Sc. Per Berggren, head of department, and M.Sc. Hans Engelbert for their guidance and advise, and Bo Svilling for valuable help with the experimental tests.

Contents

1. Notation

A	Matrix
B	Vector
c	Viscous damping
F	Force
h	Height
J	Moment of inertia
k	Spring stiffness
L	Length
M	Torque
m	Mass
p	Gear ratio
Q	Generalised force
q	Generalised co-ordinate
r	Radius
T	Kinetic energy
t	Time
V	Potential energy
v	Velocity
v	Velocity vector
x	Displacement co-ordinate
x	Displacement vector
β	Angle
θ	Rotational angle co-ordinate
ω	Angular velocity

Indices

e	Engine
s	Soil
t	Tamper

2. Introduction

Compaction is a vital part of many building and civil engineering projects. The purpose is to improve the load capacity of a fill by increasing the density of the fill material. This is achieved through the application of external forces.

The quality of the compaction has a decisive influence on the safety and lifetime of the final construction. In for example road construction, compaction makes the soil better capable to withstand the loads of traffic and diminishes the risk of future settlement. This means that maintenance costs are considerably reduced.

Though compaction plays this important role, its costs represent only a small share of the total construction costs, normally less than five per cent.

Fill material vary from clay with particles smaller than 0,002 mm, up to rock fill with blocks one meter or more in size. Fills containing waste products are becoming increasingly common.

It is customary to classify compaction with respect to the frequency of the applied load. *Static loading* has zero frequency, *Impact loading* has a low frequency, up to some tens of Hz, and for higher frequency it is called *Dynamic loading*.

The tamping machine of this work, shown in figure 5.1, operates at a frequency of approximately 12 Hz. This impact compaction machine is a product of Svedala Compaction Equipment AB, Karlskrona, Sweden.

So far it has been developed using experience of design engineers and testing in practice. The company now considers a better fundamental understanding of the dynamic behaviour of the machine to be crucial for further product development.

The only work that is found in the literature about this type of machines is that of Mohsin [1]. He studied an Electro-tamper for different kinds of soils and presented a theoretical model of the dynamic behaviour.

The aim of this work is to develop a theoretical model of the dynamic behaviour of the Petrol-tamper LT 70 of Svedala Compaction Equipment AB. The model will contain essential design parameters to facilitate the study of their influence during product development. An experimental investigation will be performed to obtain necessary information about certain parameters and for verification of the theoretical model.

3. Theoretical Model

3.1 Simplifications

The tamper is simplified into the theoretical model of figure 3.1 and figure 3.2. It is divided into three main parts, represented by lumped masses m_1 = 19,7 kg, m_2 = 3,9 kg, and m_3 = 46,5 kg. Lumping details are presented in appendix A.

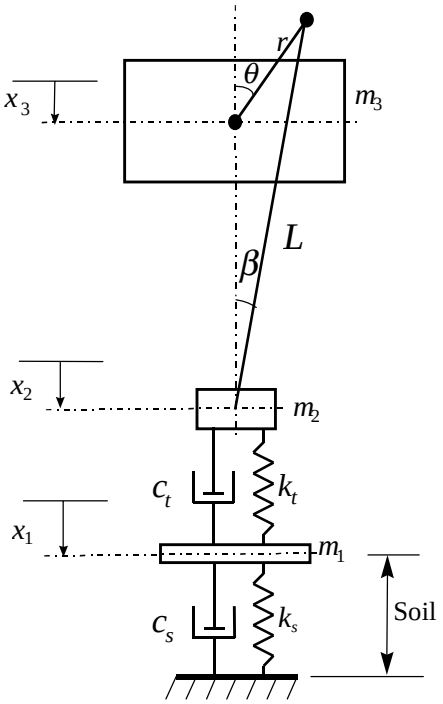

Figure 3.1. Simplified tamper model.

The soil to be compacted is complicated to model in an actual case. Models consisting of combinations of springs and dampers have been suggested by Adam [2] and Bathelt [4]. Mohsin [1] uses the model of Bathelt [4] and

states that the influence of soil constants on the dynamic behaviour of the tamper is small.

Whether this is generally valid, as well as a further study of soil models, are beyond the scope of this work. The simulated soil in our experimental investigation is a viscoelastic polymer, assumed possible to represent by a spring, k_s, and a damper, c_s, according to figure 3.1.

Other soil representations, using for example the work of Adam [2], can easily be introduced into the equations of the next section when necessary for further studies.

The force between m_1 and m_2 is primarily transmitted by the spring, k_t. Some viscous damping, c_t, is also present, since lubricating oil is pressed through channels in the inner tube during a stroke. The magnitude of this damping constant is the most uncertain value of our model.

The determination of spring constants k_s = 13280 N/m and k_t = 77 N/m is described in appendix B.

The determination of damping constants c_s = 55,6 N/m and c_t = 496 Ns/m is described in appendix C.

The motions of mass m_1, m_2 and m_3 are measured by co-ordinates x_1, x_2 and x_3 respectively, relative to a fixed co-ordinate system. Only vertical tamping movements are assumed. This means that the foot angle of 12°, that makes the tamper move forward during actual operation, is neglected.

Zero level of x_1 is at stationary level, x_0, of the tamper foot. Zero level of x_2 is the zero level of x_1 plus the distance to mid position of the piston in the inner tube. Zero level of x_3 is the zero level of x_2 plus the length of the connecting rod, L = 416 mm, minus the radius, r = 27,5 mm, of the gear wheel connection. Consequently, when x_3 is zero angles β and θ are zero.

The rotating disc shown in figure 3.2 actually consists of several parts, including the inertia of the engine. Details on the replacement of these parts into this equivalent single disc of mass moment of inertia, J = 0,598 kgm^2, are described in appendix D. Variation of J with θ, due to varying moment arm to for example the piston mass, is neglected.

The variation of the engine torque, for the relatively small variations in angular velocity expected, is neglected. Performance curves of the engine is given in appendix E.

The mean operational angular velocity of J is approximately 77 s^{-1}. With gear ratio p = 6,272 this gives an angular velocity of the engine of approximately 4600 rpm. Consequently the torque, M = 41,83 Nm, acting on the inertia, J, is assumed to be constant.

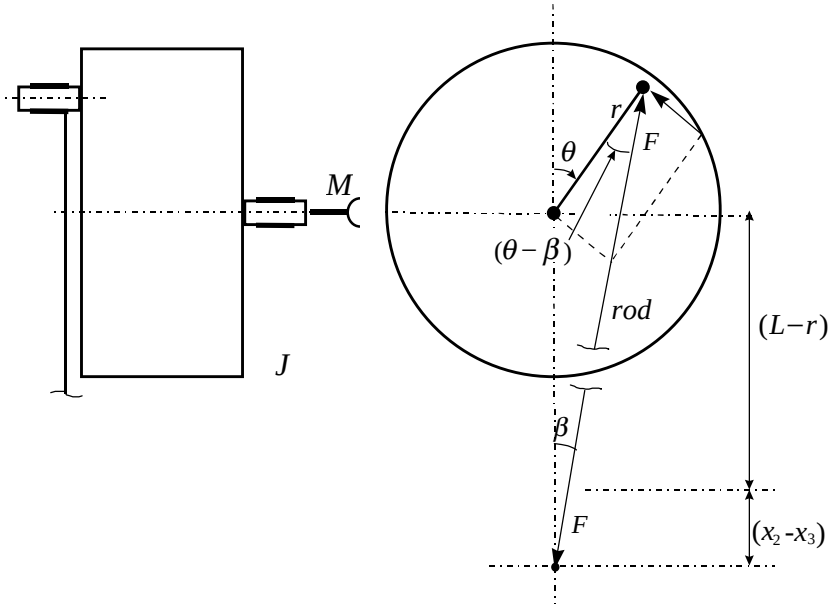

Figure 3.2. Equivalent single rotating disc.

Because of the large ratio of L over r the angle between the connecting rod and the vertical, β, is very small. In the following it is set to zero. This implies that the force in the rod, F, is approximately vertical.

3.2 Equations of motion by Newton's Method

Applying Newton's second law on the masses in figure 3.1 the equations of translational motion become

$$c_t(\dot{x}_2 - \dot{x}_1) + k_t(x_2 - x_1) - c_s\dot{x}_1 - k_s(x_1 + x_0) + m_1 g = m_1\ddot{x}_1 \tag{3.1}$$

$$F - c_t(\dot{x}_2 - \dot{x}_1) - k_t(x_2 - x_1) + m_2 g = m_2\ddot{x}_2 \tag{3.2}$$

$$-F + m_3 g = m_3\ddot{x}_3 \tag{3.3}$$

Using the assumption of constant J, the equation of rotational motion of the disc in figure 3.2 becomes

$$M - Fr\sin\theta = J\ddot{\theta} \tag{3.4}$$

The kinematic relation between m_2 and m_3 is

$$x_2 = x_3 - r\cos\theta + r \tag{3.5}$$

$$\dot{x}_2 = \dot{x}_3 + r\dot{\theta}\sin\theta \tag{3.6}$$

$$\ddot{x}_2 = \ddot{x}_3 + r\ddot{\theta}\sin\theta + r\dot{\theta}^2\cos\theta \tag{3.7}$$

For shorter notation we introduce

$$\begin{cases} s = \sin\theta \\ w = \cos\theta \end{cases} \tag{3.8}$$

Finally, combining equation 3.1 through 3.8 and eliminating F and x_2, the equations of motion for x_1, x_3, and θ become

$$\begin{aligned} m_1\ddot{x}_1 &= -(c_t + c_s)\dot{x}_1 + c_t\dot{x}_3 + c_t rs\dot{\theta} - (k_t + k_s)x_1 \ldots \\ &\ldots + k_t x_3 - k_t rw + k_t r - k_s x_0 + m_1 g \end{aligned} \tag{3.9}$$

$$m_2\ddot{x}_3 + \ddot{\theta}\left(\frac{J}{rs} + m_2 rs\right) = c_t\dot{x}_1 - c_t\dot{x}_3 - m_2 rw\dot{\theta}^2 - c_t rs\dot{\theta} \ldots$$
$$\ldots + k_t x_1 - k_t x_3 + k_t rw - k_t r + m_2 g + \frac{M}{rs} \tag{3.10}$$

$$m_3\ddot{x}_3 - \frac{J\ddot{\theta}}{rs} = m_3 g - \frac{M}{rs} \tag{3.11}$$

This system of three coupled non-linear ordinary differential equations describes the dynamic behaviour of the tamper.

3.3 Equations of motion by Lagrange's Method

An alternative way to derive the equations of motion is to use Lagrange's equations

$$\frac{d}{dt}\left(\frac{dT}{d\dot{q}_i}\right) - \frac{dT}{dq_i} + \frac{dV}{dq_i} = Q_i \tag{3.12}$$

where T is the kinetic energy and V is the potential energy of the system, and q_i are generalised co-ordinates and Q_i are non-conservative generalised forces.

The basic difference compared to Newton's method is the use of scalar quantities work and energy, instead of vector quantities force and displacement. The advantage is that constraint forces do not have to be considered explicitly and then eliminated, in this case the force F.

The total kinetic energy of the system is

$$T = \frac{m_1\dot{x}_1^2}{2} + \frac{m_2\dot{x}_2^2}{2} + \frac{m_3\dot{x}_3^2}{2} + \frac{J\dot{\theta}^2}{2} \tag{3.13}$$

Using equation 3.6 this can be rewritten as

$$T = \frac{m_1 \dot{x}_1^2}{2} + \frac{m_2 (\dot{x}_3 + r\dot{\theta}\sin\theta)^2}{2} + \frac{m_3 \dot{x}_3^2}{2} + \frac{J\dot{\theta}^2}{2} \tag{3.14}$$

The total potential energy of the system is

$$V = \frac{k_s (x_1 + x_0)^2}{2} + \frac{k_t (x_2 - x_1)^2}{2} - m_1 g x_1 - m_2 g x_2 - m_3 g x_3 \tag{3.15}$$

Using equation 3.5 this can be rewritten as

$$V = \frac{k_s (x_1 + x_0)^2}{2} + \frac{k_t (x_3 - r\cos\theta + r - x_1)^2}{2} - m_1 g x_1 \ldots$$
$$- m_2 g (x_3 - r\cos\theta + r) - m_3 g x_3 \tag{3.16}$$

The parts on the left-hand side of equation 3.12, using $q_1 = x_1$, $q_2 = x_3$, and $q_3 = \theta$ as generalised co-ordinates, become

$$\frac{dT}{d\dot{x}_1} = m_1 \dot{x}_1 \tag{3.17}$$

$$\frac{dT}{d\dot{x}_3} = m_2 \dot{x}_3 + m_2 r\dot{\theta}\sin\theta + m_3 \dot{x}_3 \tag{3.18}$$

$$\frac{dT}{d\dot{\theta}} = m_2 r\dot{x}_3 \sin\theta + m_2 r^2 \dot{\theta}\sin^2\theta + J\dot{\theta} \tag{3.19}$$

$$\frac{d}{dt}\left(\frac{dT}{d\dot{x}_1}\right) = m_1 \ddot{x}_1 \tag{3.20}$$

$$\frac{d}{dt}\left(\frac{dT}{d\dot{x}_3}\right) = (m_2 + m_3)\ddot{x}_3 + m_2 r\ddot{\theta}\sin\theta + m_2 r\dot{\theta}^2\cos\theta \tag{3.21}$$

$$\frac{d}{dt}\left(\frac{dT}{d\dot{\theta}}\right) = m_2 r\ddot{x}_3 \sin\theta + m_2 r\dot{x}_3\dot{\theta}\cos\theta + m_2 r^2\ddot{\theta}\sin^2\theta \ldots$$
$$\ldots + 2m_2 r^2\dot{\theta}^2 \sin\theta\cos\theta + J\ddot{\theta} \tag{3.22}$$

$$\frac{dT}{dx_1} = 0 \tag{3.23}$$

$$\frac{dT}{dx_3} = 0 \tag{3.24}$$

$$\frac{dT}{d\theta} = m_2 \dot{x}_3 r\dot{\theta}\cos\theta + m_2 r^2 \dot{\theta}^2 \sin\theta\cos\theta \tag{3.25}$$

$$\frac{dV}{dx_1} = (k_s + k_t)x_1 + k_s x_0 - k_t x_3 + k_t r\cos\theta - k_t r - m_1 g \tag{3.26}$$

$$\frac{dV}{dx_3} = -k_t x_1 + k_t x_3 - k_t r\cos\theta + k_t r - m_2 g - m_3 g \tag{3.27}$$

$$\begin{aligned}\frac{dV}{d\theta} &= -k_t x_1 r\sin\theta + k_t x_3 r\sin\theta - k_t r^2 \sin\theta\cos\theta \ldots \\ &\ldots + k_t r^2 \sin\theta - m_2 g r\sin\theta\end{aligned} \tag{3.28}$$

The generalised non-conservative forces on the right-hand side of equation 3.12 are

$$Q_i = \sum_{k=1}^{3} F_k \frac{\partial x_k}{\partial q_i} + M\frac{\partial\theta}{\partial q_i} \tag{3.29}$$

giving

$$Q_1 = -c_s \dot{x}_1 - c_t(\dot{x}_1 - (\dot{x}_3 + r\dot{\theta}\sin\theta)) \tag{3.30}$$

$$Q_2 = -c_t(\dot{x}_3 + r\dot{\theta}\sin\theta - \dot{x}_1) \tag{3.31}$$

$$Q_3 = M - c_t(\dot{x}_3 + r\dot{\theta}\sin\theta - \dot{x}_1)r\sin\theta \tag{3.32}$$

Inserting the parts into equation 3.12 gives

$$\begin{aligned}&m_1\ddot{x}_1 + (k_s + k_t)x_1 + k_s x_0 - k_t x_3 + k_t r\cos\theta \ldots \\ &\ldots - k_t r - m_1 g = -c_s \dot{x}_1 - c_t(\dot{x}_1 - (\dot{x}_3 + r\dot{\theta}\sin\theta))\end{aligned} \tag{3.33}$$

$$(m_2 + m_3)\ddot{x}_3 + m_2 r\ddot{\theta}\sin\theta + m_2 r\dot{\theta}^2\cos\theta - k_t x_1 + k_t x_3 \ldots$$
$$\ldots - k_t r\cos\theta + k_t r - m_2 g - m_3 g = -c_t(\dot{x}_3 + r\dot{\theta}\sin\theta - \dot{x}_1) \quad (3.34)$$

$$m_2 r\ddot{x}_3\sin\theta + m_2 r^2\ddot{\theta}\sin^2\theta + m_2 r^2\dot{\theta}^2\sin\theta\cos\theta + J\ddot{\theta}\ldots$$
$$\ldots - k_t x_1 r\sin\theta + k_t x_3 r\sin\theta - k_t r^2\sin\theta\cos\theta + k_t r^2\sin\theta\ldots \quad (3.35)$$
$$\ldots - m_2 g r\sin\theta = M - c_t(\dot{x}_3 + r\dot{\theta}\sin\theta - \dot{x}_1)r\sin\theta$$

Rearranging equation 3.33 through 3.35, using also equation 3.8, gives

$$m_1\ddot{x}_1 = -(c_t + c_s)\dot{x}_1 + c_t\dot{x}_3 + c_t rs\dot{\theta} - (k_t + k_s)x_1 \ldots$$
$$\ldots + k_t x_3 - k_t rw + k_t r - k_s x_0 + m_1 g \quad (3.36)$$

$$m_2\ddot{x}_3 + \ddot{\theta}\left(\frac{J}{rs} + m_2 rs\right) = c_t\dot{x}_1 - c_t\dot{x}_3 - m_2 rw\dot{\theta}^2 - c_t rs\dot{\theta}\ldots$$
$$\ldots + k_t x_1 - k_t x_3 + k_t rw - k_t r + m_2 g + \frac{M}{rs} \quad (3.37)$$

$$m_3\ddot{x}_3 - \frac{J\ddot{\theta}}{rs} = m_3 g - \frac{M}{rs} \quad (3.38)$$

which are, of course, the same as equation 3.9 through 3.11.

4. Solution Method

4.1 Marching Procedure

Since the equations of motion are non-linear the most straightforward way of solving them is by a marching procedure. Using matrix notation we have

$$\mathbf{A}\ddot{\mathbf{x}} = \mathbf{B} \tag{4.1}$$

where

$$\mathbf{A} = \begin{bmatrix} m_1 & 0 & 0 \\ 0 & m_2 & \dfrac{J}{rs} + m_2 rs \\ 0 & m_3 & -\dfrac{J}{rs} \end{bmatrix} \tag{4.2}$$

$$\mathbf{x} = \begin{bmatrix} x_1 \\ x_3 \\ \theta \end{bmatrix} \tag{4.3}$$

$$\mathbf{B} = \begin{bmatrix} -(c_t + c_s)\dot{x}_1 + c_t\dot{x}_3 + c_t rs\dot{\theta} - (k_t + k_s)x_1 \ldots \\ \ldots + k_t x_3 - k_t rw + k_t r - k_s x_0 + m_1 g \\ \\ c_t\dot{x}_1 - c_t\dot{x}_3 - m_2 rw\dot{\theta}^2 - c_t rs\dot{\theta} \ldots \\ \ldots + k_t x_1 - k_t x_3 + k_t rw - k_t r + m_2 g + \dfrac{M}{rs} \\ \\ m_3 g - \dfrac{M}{rs} \end{bmatrix} \tag{4.4}$$

The second order system of equation 4.1 is transformed into a first order system by introducing

$$\dot{\mathbf{x}} = \begin{bmatrix} v_1 \\ v_3 \\ \omega \end{bmatrix} = \mathbf{v} \tag{4.5}$$

and writing

$$\begin{bmatrix} \dot{\mathbf{x}} \\ \dot{\mathbf{v}} \end{bmatrix} = \begin{bmatrix} \mathbf{v} \\ \mathbf{A}^{-1}\mathbf{B} \end{bmatrix} \tag{4.6}$$

This initial value problem of six first order equations is solved by the Runga-Kutta method.

As initial values of displacements and velocities experimental values at one point of time are used. The agreement between the marched out solution and measured values at other times then indicates the correctness of the theoretical model.

Because of the stationary cyclic operation it is only necessary to study one oscillation. This also implies that the values at the end of the cycle must be the same as the initial values.

The results are shown in chapter six together with the experimental results.

5. Experimental Investigation

5.1 Experimental Set-up

To verify the theoretical model an experimental investigation was done at the laboratory of Svedala Compaction Equipment AB. A tamper LT70 was rigged as shown in figure 5.1.

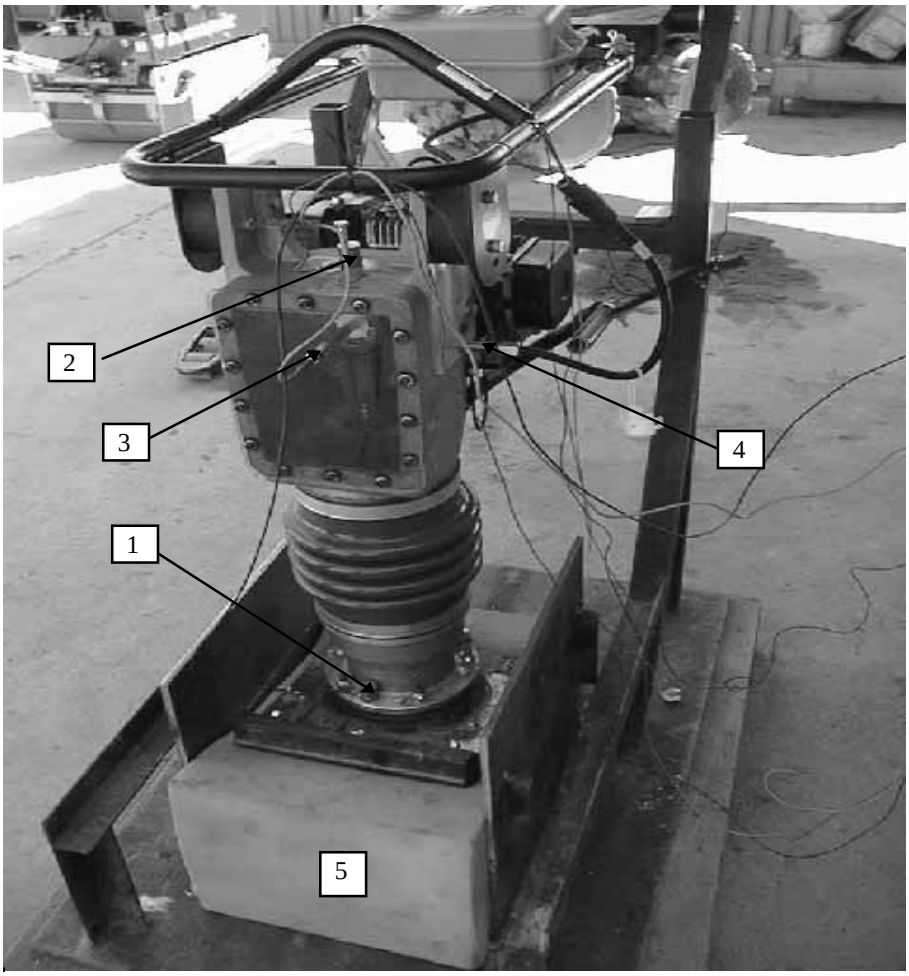

Figure 5.1. Photo of the experimental set-up.

The Tamper was supported horizontally by a steel structure through rubber elements, allowing it to move in the vertical direction only. As soil replacement a soft, elastic material (figure 5.1, item 5) was used. The spring stiffness of this material was established experimentally. This is described in appendix B.

Four different signals of data were collected from each test run (figure 5.1, item 1-4).

1. Accelerometer for accelerations of m_1.
2. Accelerometer for accelerations of m_3.
3. Magnetic field sensor for indication of the connecting rod angle.
4. Magnetic field sensor for indication of angular velocity.

Item 3 and 4 needs further explanation. To establish $\theta(t)$ a reference point has to be measured. Every time the connecting rod passes the top of its orbit it passes through a magnetic field and a signal, in form of a square wave pulse, is indicated. Combining this signal with the signal from item 4 the function $\theta(t)$ is known.

The signal from item 4 is measured in the same way as in item 3 but the indicator is placed so that a pulse is obtained every time a cog of the gearwheel passes it. Knowing the sampling time the angular velocity function can be calculated.

Three test runs were done at full speed of the tamper. Through a transmitter, Brüel & Kjær Charge Amplifier Type 2635, the signal was integrated to obtain displacement and velocity from the values of acceleration from the accelerometers. The results are shown in chapter six together with the theoretical results.

6. Theoretical and Experimental Results

6.1 Results

In figures 6.1 through 6.6 below results from the experimental test are shown by dot-dashed lines. The calculated values from the theoretical model are shown by solid lines.

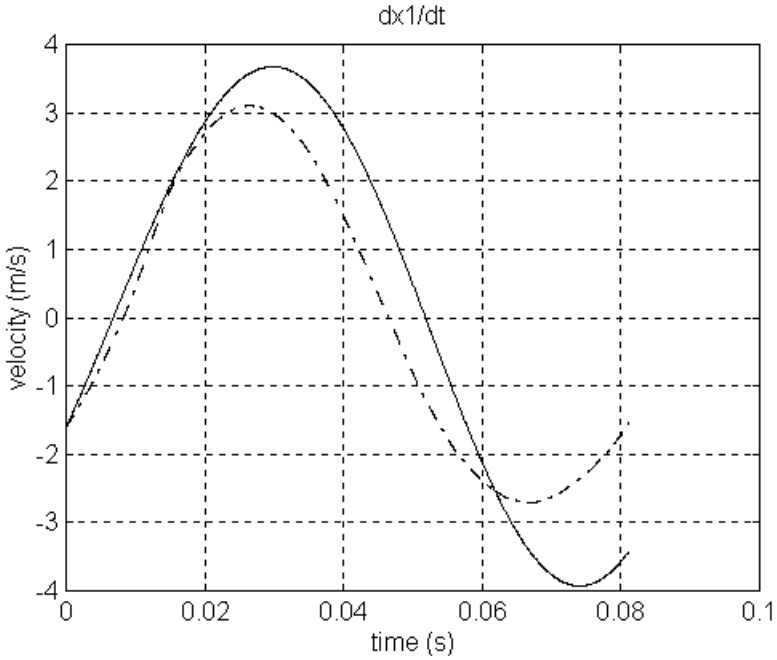

Figure 6.1. Velocity of m_1, measured and calculated values.

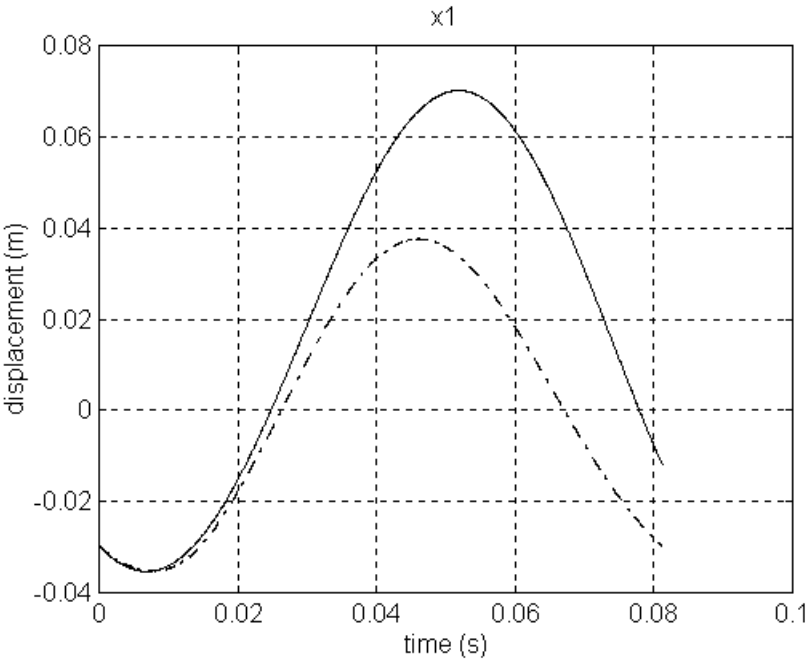

Figure 6.2. Displacement of m_1, measured and calculated values.

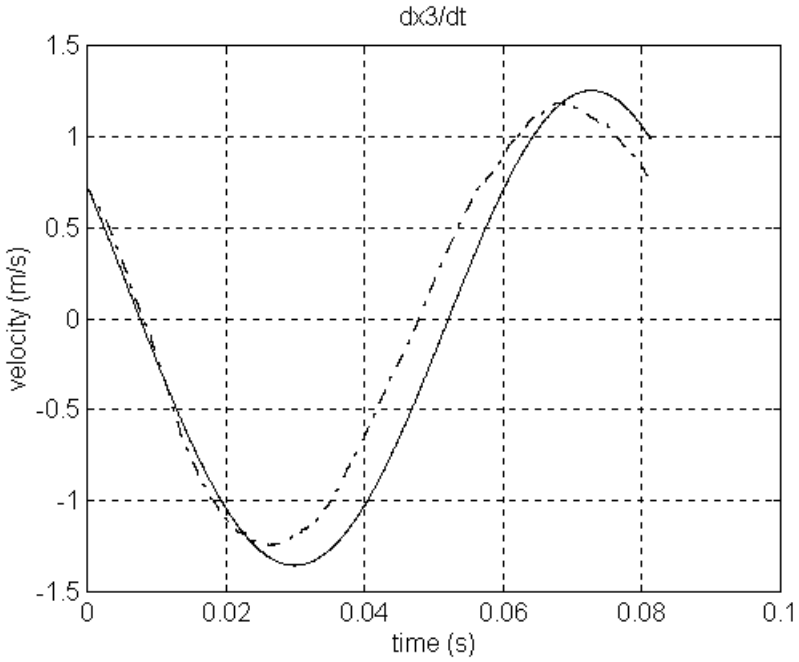

Figure 6.3. Velocity of m_3, measured and calculated values.

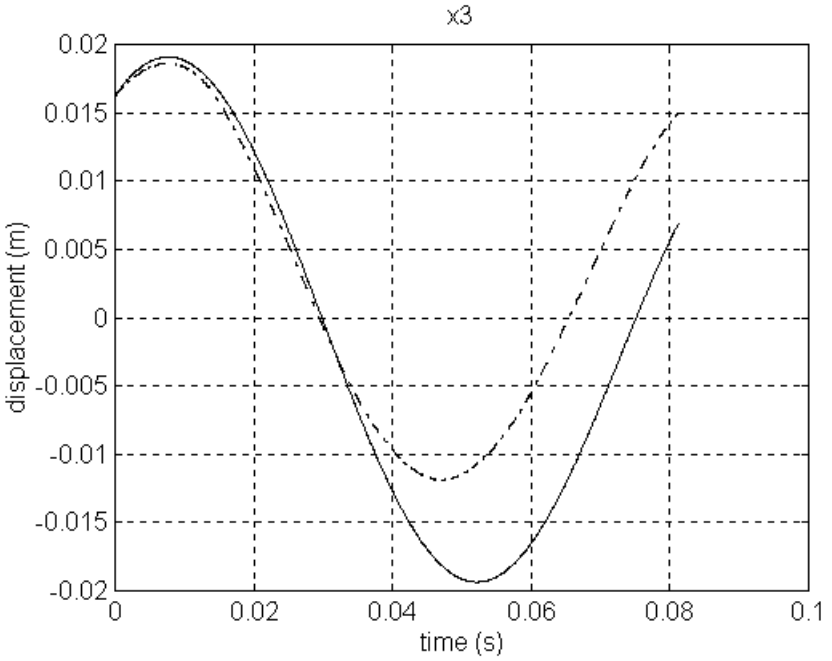

Figure 6.4. Displacement of m_3, measured and calculated values.

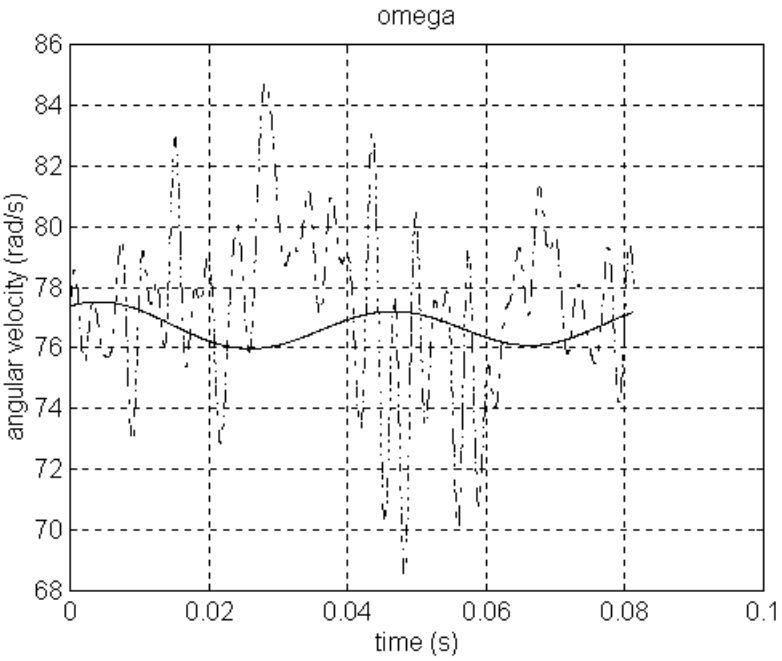

Figure 6.5. Angular velocity, measured and calculated values.

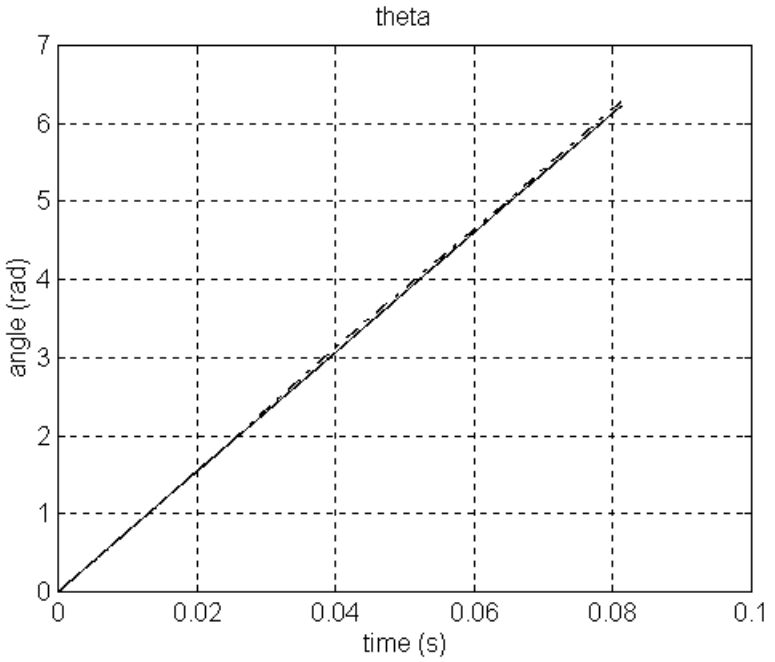

Figure 6.6. Rotational angle, measured and calculated values.

6.2 Discussion

The agreement between calculated and measured values is not quite satisfactory. To rule out the solution method itself as a possible source of this discrepancy, for example by accumulation of numerical errors during the marching procedure, equation 4.1 is solved using measured values of velocities and displacements in the right-hand side.

If in this case the result differ from measured accelerations, this difference cannot be due to accumulation of numerical errors.

The results are shown in figure 6.7 and 6.8, where bold lines show calculated values.

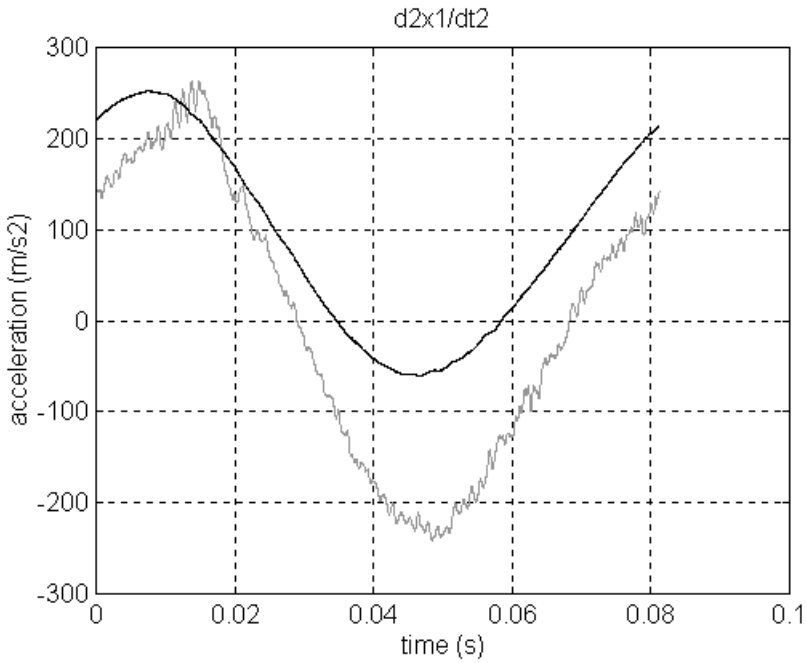

Figure 6.7. Acceleration of m_1, calculated values (using measured values of velocities and displacements in the right-hand side of equation 4.1 at each time) and measured values.

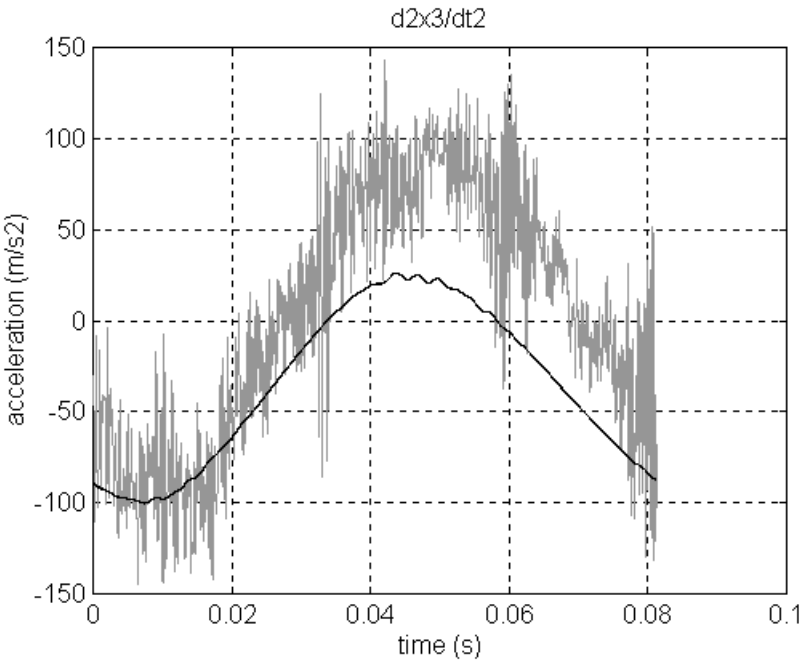

Figure 6.8. Acceleration of m_3, calculated values (using measured values of velocities and displacements in the right-hand side of equation 4.1 at each time) and measured values.

From figures 6.7 and 6.8 we can conclude that the numerical solution method is not responsible for the discrepancy between calculated and measured values in figures 6.1 through 6.6.

The difference is instead most likely due to uncertainties in the damping constants of the model. A more accurate determination of damping constants, by a more extensive experimental investigation, is therefore suggested as a continuation of this work.

Other possible, but probably minor, sources for the difference are the choice of how to lump the masses and that the angle θ and angular velocity $\dot{\theta}$ are difficult to measure accurately.

7. Conclusions

The subject of this work was to study the dynamic behaviour of the petrol tamper LT70 of Svedala Compaction Equipment AB. A theoretical model was suggested and equations of motion were derived by Newton's and Lagrange's method. A computer program was developed to solve the resulting system of non-linear differential equations.

To verify the theoretical model and to obtain necessary information about certain parameters an experimental investigation was carried out. The agreement between calculated and experimental values is not quite satisfactory.

The difference is most likely due to uncertainties in the damping constants of the model. For a more accurate determination of the damping constants a more extensive experimental investigation must be done. Because of limitations in time we decided not to include this in our work but suggests it as a first step in a continued investigation by others.

Although the theoretical model does not yet agree completely with measured results, this work has significantly increased the knowledge at Svedala Compaction Equipment AB about the dynamic behaviour of the tamper. This will certainly be beneficial to further product development.

8. References

1. Mohsin, S.: *Investigation of the Dynamic Behaviour of Tamping Systems*, Baumaschine und Bautechnik-14.Jahrgang, Heft 1, Januar, 1967.
2. Adam, D.: *Flächendeckende dynamische verdichtungskontrolle* (FDVK) *mit vibrationswalzen*, Fakultät für Bauingenieurwesen, Technischen Universität Wien, 1996.
3. Inman, D.: *Engineering Vibration*, Prentice Hall, 1996.
4. Bathelt, U.: *Das Arbeitsverhalten des Rüttelverdichters auf plastisch-elastischem Untergrund*, Bautechnik-Archiv, Heft 12, Berlin, 1956.

A. Determination of Masses

The tamper LT70 is divided in to three lumped masses.

	$\mathbf{m_1}$	
1	Spring	1,6
1	Bellows bracket	2,1
1	Plastic stop	0,35
2	Slider	0,09
1	Inner tube	5,9
1	Foot	8,0
1	Cover	0,6
	Sum	**19,73 kg**

	$\mathbf{m_2}$	
1	Piston	0,5
1	Connecting rod	1,7
1	Piston bolt	0,09
1	Spring	1,6
	Sum	**3,89 kg**

	$\mathbf{m_3}$	
1	Engine etc.	46,4
1	Slider	0,09
	Sum	**46,49 kg**

B. Determination of Spring stiffness

B.1 Spring Stiffness for the Soil Replacement

The spring stiffness (k_s) of the soil replacement was established experimentally. The static deflection of the material was measured for six different loads. Using linear regression the spring stiffness (k_s) becomes 13280 N/m.

B.2 Spring stiffness for the Tamper

Using data from the spring supplier the spring stiffness is seen to be 38,5 kN/m. As there are two springs working according to figure B.2, we multiply the spring stiffness by two and k_t becomes 77 kN/m.

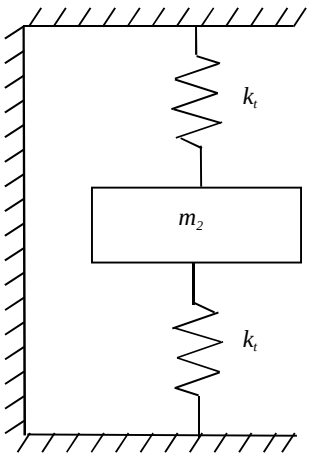

Figure B.2. Spring system of the tamper.

C. Determination of Damping Constants

The damping coefficient in the soil replacement was determined by modal analysis. A mass, m_s=13 kg with an Area, A_s=0,0415 m^2, was placed on the top of the soil material and excited by an impulse hammer.

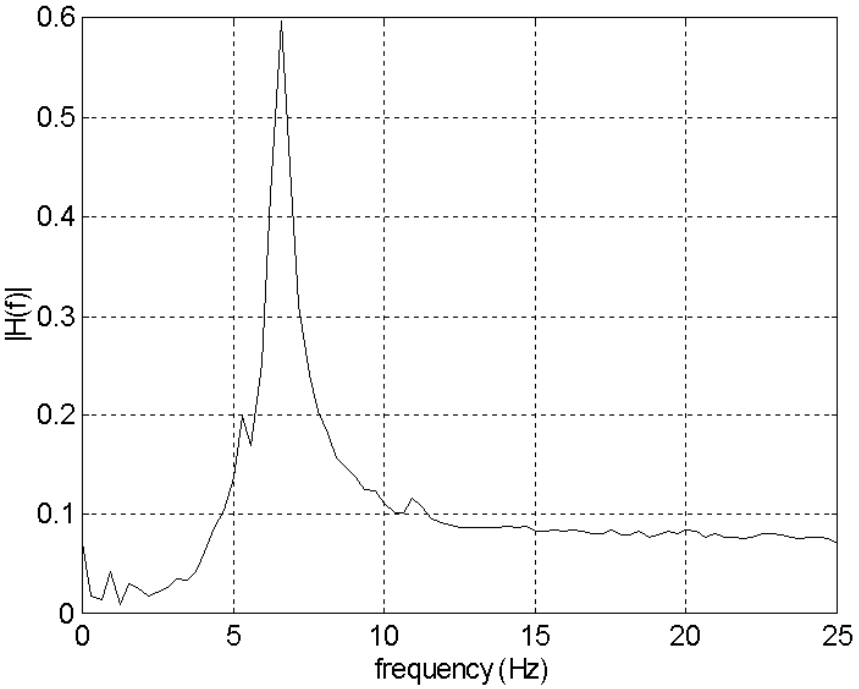

Figure C.1. Frequency Response.

From the Transmissibility function we can calculate the non-dimensional coefficient, ζ_s, for the soil as

$$\zeta_s = \frac{f_b - f_a}{2 \cdot f_d} \tag{C.1}$$

With $\left|H(f_d)\right| = 0{,}5958$, $f_d = 6{,}5625\,\text{Hz}$, and

$$|H(f_a)| = |H(f_b)| = \frac{|H(f_d)|}{\sqrt{2}} = \frac{0{,}5958}{\sqrt{2}} = 0{,}4213 \qquad \text{(C.2)}$$

we get $f_a = 6{,}245$ Hz, $f_b = 6{,}925$ Hz, giving

$$\zeta_s = \frac{f_b - f_a}{2 \cdot f_d} = \frac{6{,}925 - 6{,}245}{2 \cdot 6{,}5625} = 0{,}0518 \qquad \text{(C.3)}$$

The damping constant, c_s, then becomes

$$c_s = 2\zeta_s \sqrt{\frac{A_{m_1}}{A_s} k_s m_s} \qquad \text{(C.4)}$$

where A_{m_1} is the area of the tamper foot used when the stiffness of the soil was determined.

Inserting values gives

$$c_s = 2 \cdot 0{,}05 \sqrt{\frac{0{,}0742}{0{,}0415} \cdot 13280 \cdot 13} = 55{,}6 \quad \text{Ns/m} \qquad \text{(C.5)}$$

The tamper itself also has viscous damping. One way of finding out the magnitude of this is to make a modal analysis. In this work however we will estimate the damping constant in a simplified way.

Assuming that displacement x_2 is possible to describe approximately as

$$x_2 = X_2 \cos \omega t \qquad \text{(C.6)}$$

the stationary solution of equation 3.1 will principally be

$$x_1 = X_1 \cos(\omega t - \varphi) + const \qquad \text{(C.7)}$$

By insertion into equation 3.1 the quota of X_1 over X_2 can then be shown to be

$$\frac{X_1}{X_2} = \sqrt{\frac{{c_t}^2\omega^2 + {k_t}^2}{{c_t}^2\omega^2 + 2 \cdot c_t c_s \omega^2 + {c_s}^2\omega^2 + (k_t + k_s - m_1\omega^2)^2}} \tag{C.8}$$

Now, by putting X_1 equal to the measured amplitude of x_1, X_2 equal to the measured amplitude of x_2, and ω equal to the measured mean angular velocity, we get

$$c_t = 346 \text{ Ns/m} \tag{C.9}$$

D. Determination of Moments of Inertia

Figure D.1 shows a complete model of the moving parts of the engine, and the equivalent single disc included in the model described in chapter 3.

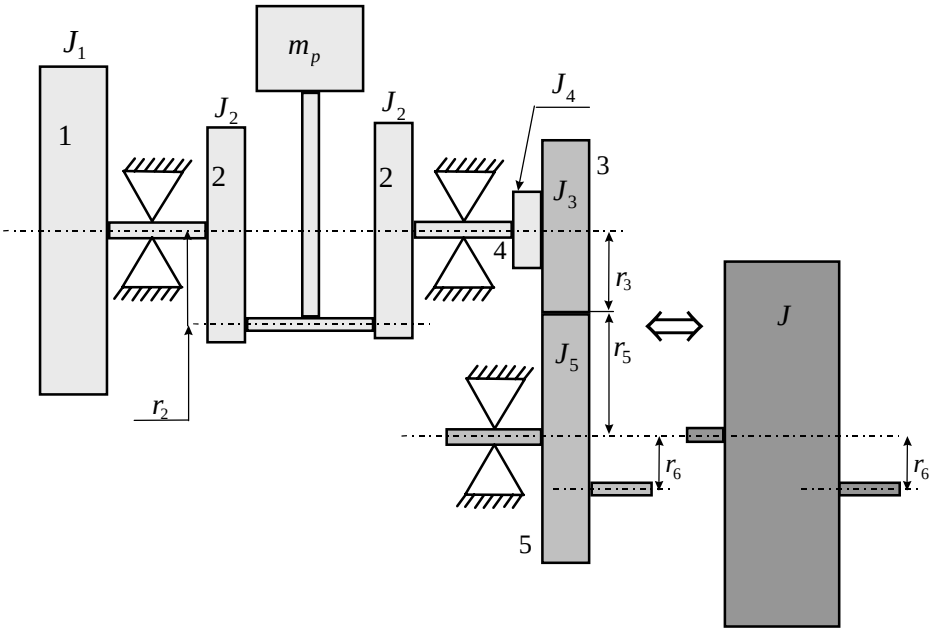

Figure D.1. Moment of inertia replacement.

The parts are:

J = Moment of inertia of the equivalent single disc

J_e = Moment of inertia of the engine parts

J_1 = Moment of inertia of the flywheel (1)

J_2 = Moment of inertia of the crankshaft (2)

J_3 = Moment of inertia of the intermediate wheel (3) = $0{,}893 \cdot 10^{-3}\,\mathrm{kgm}^2$

J_4 = Moment of inertia of the centrifugal clutch (4)

J_5 = Moment of inertia of the gear wheel (5) = $6{,}050 \cdot 10^{-3}\,\mathrm{kgm}^2$

r_2 = Radius of the crankshaft

r_3 = Radius of the intermediate wheel = 0,0113 m

r_5 = Radius of the gear wheel = 0,07143 m

r_6 = Eccentricity = 0,0275 m

m_p = Piston mass

$$p = \text{Gear ratio} = \frac{r_5}{r_3} = 6{,}27 \qquad \text{(D.1)}$$

The moment of inertia of all engine parts except 3 and 5 was determined experimentally as follows.

A mass, m = 3,085 kg, attached to a flexible string that is rolled up around the clutch disc (4), was dropped from a height, h = 0,863 m, according to figure D.2.

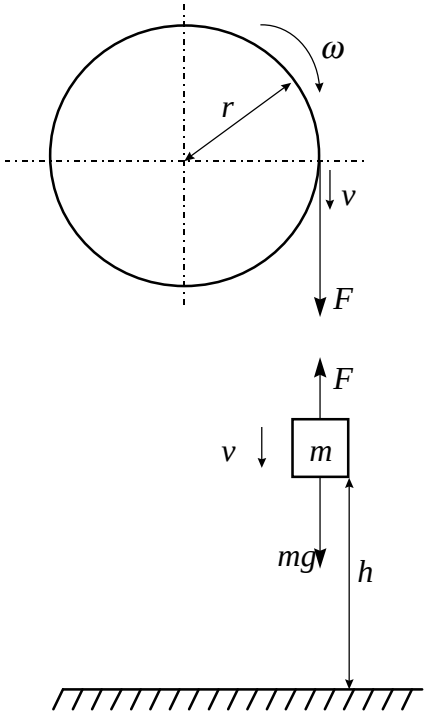

Figure D.2. Experimental determination of moment of inertia.

Mean value of the fall in twelve measurements was

$$v_{measured} = 2{,}09 \text{ m/s}$$

Conservation of energy gives

$$\frac{J_e \omega^2}{2} + \frac{m v_{measured}^{\ 2}}{2} = mgh \tag{D.2}$$

$$\omega = \frac{v_{measured}}{r_4} \tag{D.3}$$

$$J_e = \frac{2r^2}{v_{measured}^{\ 2}} \left(mgh - \frac{m v_{measured}^{\ 2}}{2} \right) = \frac{2 \cdot 0{,}04^2}{2{,}09^2} \left(3{,}085 \cdot 9{,}81 \cdot 0{,}863 - \frac{3{,}085 \cdot 2{,}09^2}{2} \right) = 14{,}2 \cdot 10^{-3} \text{ kgm}^2 \tag{D.4}$$

The moment of inertia of disc 3 and disc 5 are determined by the Computer Aided Design software PRO/Engineer™ after modelling the parts.

$$J_3 = 0{,}893 \cdot 10^{-3} \text{ kgm}^2 \quad \text{and} \quad J_5 = 6{,}050 \cdot 10^{-3} \text{ kgm}^2$$

Total moment of inertia of the equivalent single disc is thus

$$J = J_5 + p^2 (J_3 + J_e) \tag{D.5}$$

$$J = 6{,}050 \cdot 10^{-3} + 6{,}272^2 (0{,}893 + 14{,}2) \cdot 10^{-3} = 599{,}7 \cdot 10^{-3} \text{ kgm}^2$$

E. Performance Curves of the Engine

Engine type: ROBIN EC12

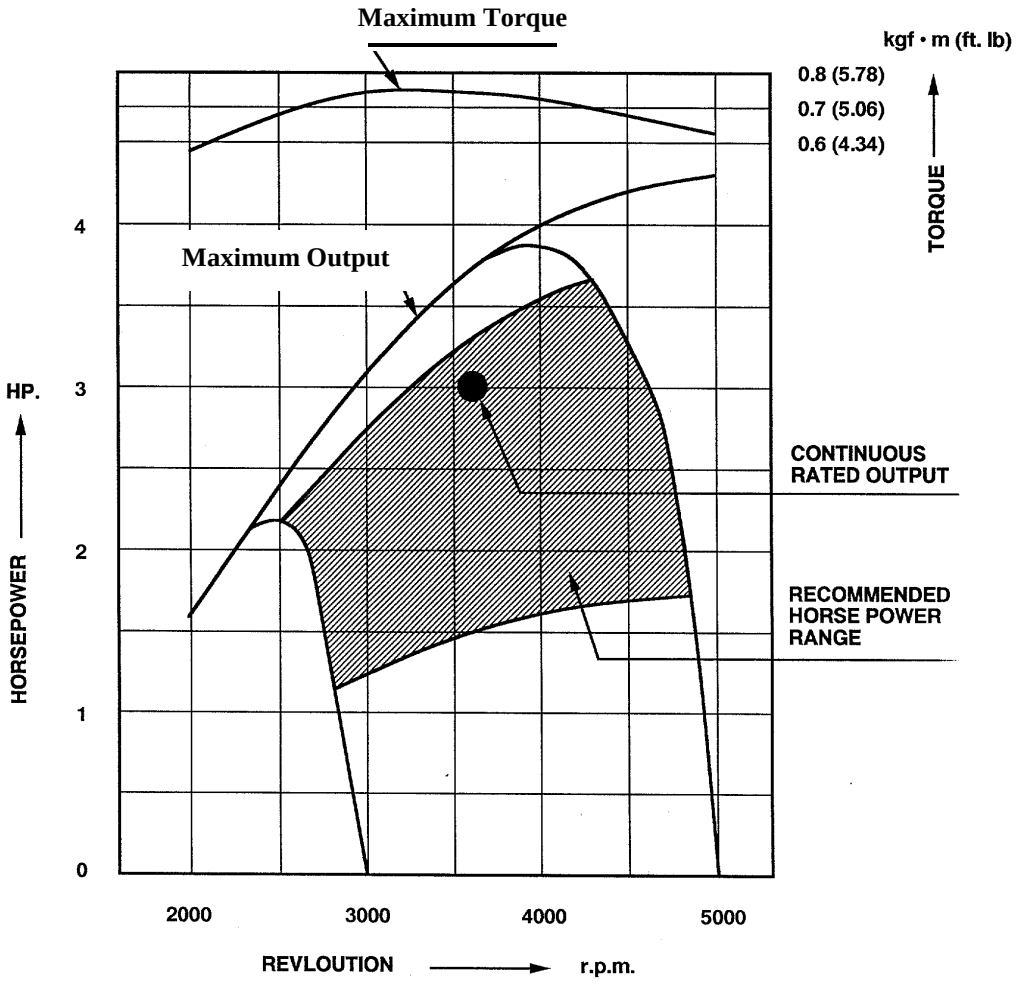

Figure E.1. Performance curves of the engine.

F. Matlab Code

```
% Headprog.m
clear
load perdata % file with measured values

%--------- Constants ----------------------------
global r g m1 m2 m3 kt ks ct cs M J
r=0.0275; g=9.81; m1=19.7; m2=3.9; m3=46.5;
kt=77.0e3; ks=13.28e3;
ct=346; cs=55.6;
M=41.83; J=0.6;

%------------- Initial values --------------------
q=1;ts=q/40000;
tf=pert1(length(pert1)); % time per cycle
x10=x1(q); x1p0=x1prim(q);
x30=x3(q); x3p0=x3prim(q);
teta0=teta(q+1); omega0=omega(1);

[t,X]=ode45('tampeq',ts,tf,[x10;x1p0;x30;x3p0;teta
0;omega0]);

%------------- Plot ------------------------------
figure(1);plot(pert1,x1,'w-.');hold
on;plot(t,X(:,1),'w');
title('x1');xlabel('time
(s)');ylabel('displacement (m)');grid on;zoom on;
figure(2);plot(pert1,x3,'w-.');hold
on;plot(t,X(:,3),'w');
title('x3');xlabel('time
(s)');ylabel('displacement (m)');grid on;zoom on;
figure(3);plot(pert1,x1prim,'w-.');hold
on;plot(t,X(:,2),'w');
title('dx1/dt');xlabel('time
(s)');ylabel('velocity (m/s)');grid on;zoom on;
figure(4);plot(pert1,x3prim,'w-.');hold
on;plot(t,X(:,4),'w');
title('dx3/dt');xlabel('time
(s)');ylabel('velocity (m/s)');grid on;zoom on;
figure(5);plot(pert1,teta,'w-.');hold
on;plot(t,X(:,5),'w');
```

```
title('theta');xlabel('time (s)');ylabel('angle
(rad)');grid on;zoom on;
figure(6);plot(pert1,omega,'w-.');hold
on;plot(t,X(:,6),'w');
title('omega');xlabel('time (s)');ylabel('angular
velocity (rad/s)');grid on;zoom on;
```

```
function xprim=tampeq(t,x);
global r g m1 m2 m3 kt ks ct cs M J % Constants

ex0=(m1+m2+m3)*g/ks;  % Static equilibrium
s=sin(x(5)); w=cos(x(5)); % substitution
A=zeros(3); % Create Matrix A
A(1,1)=m1; A(2,2)=m2; A(2,3)=J/(r*s)+m2*r*s;
A(3,2)=m3; A(3,3)=-J/(r*s);

%------------ Create Matrix B -------------------
B(1,1)=-(ct+cs)*x(2)+ct*x(4)+ct*r*s*x(6)-
(kt+ks)*x(1)+kt*x(3)-kt*r*w+kt*r+m1*g-ks*ex0;
B(2,1)=ct*x(2)-ct*x(4)-m2*r*w*x(6)^2-
ct*r*s*x(6)+kt*x(1)-kt*x(3)+kt*r*w-
kt*r+m2*g+M/(r*s);
B(3,1)=m3*g-M/(r*s);

%---------------Solving the system of equations---
X=A\B;

xprim(1)=x(2);
xprim(2)=X(1,1);
xprim(3)=x(4);
xprim(4)=X(2,1);
xprim(5)=x(6);
xprim(6)=X(3,1);
```

Department of Mechanical Engineering, Master's Degree Programme
University of Karlskrona/Ronneby, Campus Gräsvik
371 79 Karlskrona, SWEDEN

Telephone: +46 455-78016
Fax: +46 455-78027
E-mail: Goran.Broman@ima.hk-r.se